Aging and hygroscopicity variation of black carbon particles in Beijing measured by a quasi-atmospheric aerosol evolution study (QUALITY) chamber

Jianfei Peng[1, 2]*, Min Hu[1, 3]*, Song Guo[1,2], Zhuofei Du[1], Dongjie Shang[1], Jing Zheng[1], Jun Zheng[2], Limin Zeng[1], Min Shao[1], Yusheng Wu[1], Don Collins[2], Renyi Zhang[1,2]*

[1]State Key Joint Laboratory of Environmental Simulation and Pollution Control, College of Environmental Sciences and Engineering, Peking University, Beijing, China 100871

[2]Department of Atmospheric Sciences, Texas A&M University, College Station, Texas, USA 77843

[3]Beijing Innovation Center for Engineering Sciences and Advanced Technology, Peking University, Beijing, China 100871

*To whom correspondence should be addressed. E-mail: pengjianfeipku@gmail.com (Jianfei Peng); minhu@pku.edu.cn (Min Hu); renyi-zhang@geos.tamu.edu (Renyi Zhang)

Abstract. Measurements of aging and hygroscopicity variation of black carbon (BC) particles in Beijing were conducted using a 1.2 m^3 quasi-atmospheric aerosol evolution study (QUALITY) chamber, which consisted of a bottom flow chamber where ambient air was pulled through continuously and an upper reaction chamber where aging of BC particles occurred. Within the reaction chamber, transmission of the solar ultraviolet irradiation was approximately 50% - 60%, wall loss of primary gaseous pollutants was negligible compared with the replenish rate by gas exchange, and BC exhibited a half-lifetime about 3-7 hours. Typically, equilibrium for the primary gases, temperature, and relative humidity between the reaction chamber and ambient air was established within 1 hour. Rapid growth of BC particles was observed, with an average total growth of 77±33nm and average growth rate of 26±11 nm h^{-1}. Secondary organic aerosols (SOA) accounted for more than 90% of the coating mass. The O/C ratio of SOA was 0.5, lower than the ambient level. The hygroscopic growth factor of BC particles decreased slightly with an initial thin coating layer because of BC reconstruction, but subsequently increased to 1.06-1.08 upon further aging. The κ (kappa) values for BC particles and coating materials were calculated as 0.035 and 0.040 at the subsaturation and supersaturation conditions, respectively, indicating low hygroscopicity of coated SOA on BC particles. Hence, our results indicate that initial photochemical aging of BC particles does not appreciably alter the particle hygroscopicity in Beijing.

1 Introduction

Atmospheric aerosols undergo continuous and complicated transformation during their residence time in the atmosphere. The aging of aerosols is likely resulted from both physical (i.e., coagulation, condensation, equilibrium partitioning, and evaporation) and chemical (i.e., photochemical gas-phase oxidation and multi-phase reactions) processes (Zhao et al., 2006; Qiu et al., 2013; Zhang et al., 2015). Also, there are typically large variations in the particle properties (i.e., size, mass, chemical composition, morphology, and optical and hygroscopic parameters) during aging, significantly influencing the aerosol impacts on visibility, human health, weather, and climate (Jacobson, 2001; Guo et al., 2014). A better understanding of the aging process of aerosols in the atmosphere is critical in atmospheric and climate research.

For example, the scientific interest in the climate effects of black carbon (BC) has remained, since BC is the strongest absorber of visible solar radiation (Wang et al., 2013). BC solar absorption represents a central issue in climate change research, since the synthesis of satellite, in situ, and ground observations shows that the global solar absorption (direct radiative forcing or DRF) by BC is as much as 0.9 $W \cdot m^{-2}$, second only to that of CO_2 (Jacobson, 2001; Bond et al., 2013; IPCC, 2013). BC also represents an important component of air pollution for large parts of the world (Zhang et al., 2015). The properties of BC are considerably modified during aging, including the size, mass, morphology, and optical and hygroscopic parameters (Khalizov et al., 2009; Xue et al., 2009a). Enhanced light absorption of BC particles during aging not only contributes to atmospheric stabilization and exacerbation of haze formation, but also imposes large positive radiative forcing on climate (Peng et al., 2016). Furthermore, the variation in hygroscopicity during aging also regulates the lifetimes of BC particles. Hygroscopic particles serve efficiently as cloud condensed nuclei (CCN), affecting the formation, longevity and albedo of clouds (Yuan et al., 2008; Wang et al., 2011). Also, deposition of BC particles, via in-cloud scavenging and wet deposition, depends highly on the particle hygroscopicity (Bond et al., 2013). In addition, the hygroscopicity also affects the aqueous-phase reactions of atmospheric pollutants (Ervens et al., 2011; Wang et al., 2016). Previous studies using hygroscopic tandem differential mobility analyzer (H-TDMA) instruments have shown that coating of hydrophilic materials significantly increases the hygroscopic growth factor of BC particles (Saathoff et al., 2003; Khalizov et al., 2009; Guo et al., 2016). The ability of BC particles to form CCN also enhanced after coating of hydrophilic materials (Kuwata et al., 2007; Tritscher et al., 2011; Ma et al., 2013; Wittbom et al., 2014). The activation supersaturation depends on the particle size, hygroscopicity of coating materials, and the coating thickness (Ma et al., 2013). The coating materials in the previous experiments include sulfuric acid (Zhang and Zhang, 2005; Khalizov et al., 2009), oxidation products from biogenic and anthropogenic hydrocarbon species (Saathoff et al., 2003; Ma et al., 2013; Khalizov et al., 2013), or secondary organic aerosols (SOA) from single emission source (Tritscher et al., 2011). However, there still exist uncertainties for parametrization of the BC lifetime in atmospheric models, because of insufficient constraints on the hydrophobic to hydrophilic conversion of BC particles under variable ambient conditions.

Atmospheric field measurements have been performed to evaluate aging of particles on different platforms, e.g., ground, aircraft, and cruise (Moffet and Prather, 2009; DeCarlo et al.,

75 2010; Peng et al., 2014; Liu et al., 2015) and over different spatial scales (intensive
76 campaigns or long-term measurements). Typically, a wide variety of state-of art instruments
77 are employed to characterize the changes of the chemical and physical properties of aerosols.
78 On the other hand, field measurements at fixed sites are affected by transport, local emissions,
79 and chemistry, and quantification of the particle parameters during aging involves complex
80 decoupling of the various processes (Peng et al., 2016). In particular, it is challenging to
81 isolate the chemical processes from those related to meteorology (i.e., transport and mixing)
82 and emissions.

83 The methods of environmental chambers or reactors have been widely employed in
84 atmospheric chemistry research, including photochemical oxidation of volatile organic
85 compounds (VOCs) (Zhang et al., 2000), formation and growth of aerosols (Claeys, 2004;
86 Kalberer, 2004), nucleation of nanoparticles (Zhang et al., 2004; Wang et al., 2010; Zhang et
87 al., 2012), aging of BC particles (Zhang et al., 2008), and cloud formation (Ruehl et al.,
88 2016). Dependent of the scientific objectives, the designs of environmental chambers and
89 reactors vary considerably (Zhang et al., 2015). However, few of the previous experimental
90 methods have characterized the evolution of aerosols under the ambient conditions.

91 In this study, we present measurements of aging and hygroscopicity variation of BC
92 particles in Beijing using a quasi-atmospheric aerosol evolution study (QUALITY) chamber
93 (Reed, 2010; Peng et al., 2016). The performance of the QUALITY chamber for mimicking
94 the ambient gaseous concentrations (i.e., the wall loss, and gas mixing rate), ultraviolet
95 transmission, and meteorology parameters (i.e., temperature and relative humidity, RH) has
96 been evaluated.

2   Experimental method

98 The 1.2 m^3 QUALITY chamber was employed to study BC aging under ambient
99 conditions (Fig. 1). The two-layer chamber was comprised of an inner layer of 0.13 mm
100 Perfluoroalkoxy alkane (PFA) Teflon and an outer rigid 5.6 mm thick acrylic shell (Cyro
101 Industries Acrylite, OP-4). Both Acrylite OP-4 Acrylic and PFA Teflon allowed for efficient
102 ultraviolet (UV) transmission in UV-B (280-315 nm) and UV-A (315-400 nm) ranges. When
103 exposed to sunlight, the UV light transmitted through the chamber wall and initiated
104 photochemical reactions inside the chamber.

105 The two individual subdivisions of the QUALITY chamber included a bottom flow
106 chamber, where ambient air was pulled through continuously over each experiment, and an
107 upper reaction chamber, where aging of BC particles occurred (Fig. 1). The two chambers
108 were separated by a 5 μm thick semi-permeable expanded polytetrafluoroethylene (e-PTFE)
109 membrane with high degrees of chemical resistivity, microporosity, nonpolarity, and thermal
110 stability. Gaseous species penetrated the membrane by either bulk gas flow or diffusion. The
111 permeability of the e-PTFE was greater than 90 % for nearly all the tested volatile organic
112 components (Fig. S1) and other gaseous pollutants, i.e., SO_2, NO_x, O_3 and CO. Particles, on
113 the other hand, were blocked from penetration into the reaction chamber. The filtration
114 efficiency of the e-PTFE membrane was measured to be over 99.5% for particles larger than
115 15 nm. During each chamber experiment, ambient air was pulled through the flow chamber
116 continuously and gases in lower chamber permeated through the membrane into the reaction

chamber. Hence, an environment that continuously captured the ambient gas concentrations without the presence of ambient particles was created inside the reaction chamber. Since the chamber was continuously exposed to ambient gas concentrations during experiments, gases lost due to reaction, deposition or adsorption to the seed aerosols within the reaction chamber were steadily replenished by the exchange with the flow chamber. Several sampling ports were set at the side of the reaction chamber for injection of seed particles or sampling during experiment.

Seed particles were introduced in the reaction chamber via an injection line (Fig. S2). To investigate the growth of BC particles under ambient condition, monodisperse BC particles were injected into the QUALITY chamber. BC particles were generated by incomplete combustion of propane fuel in a custom-made laminar diffusion burner (Santoro et al., 1983; Qiu et al., 2012). The aerosol stream sequentially passed through a 300°C heater to evaporate the semi-volatile organic compounds in the particle phase, a Nafion dryer to remove excess moisture in the flow, and four one-meter-long cylinders containing both alumina spherules coated with potassium hypermanganate and activated carbon to remove all the gaseous pollutants (i.e., VOCs, H_2S, SO_2, NO_x, O_3). The combined measurement of particle size distribution, density and chemical composition exhibited that organics accounted for less than 10% of fresh BC mass concentration. Moreover, the single scattering albedo (SSA) of fresh BC particles was only 0.1, further confirming that few organic coatings exited on fresh BC particles after treatment. The measured removal efficiency in the cylinders for SO_2, NO and NO_2 were 99.2%, 100%, and 99.9%, respectively. The aerosol stream was then introduced through an ionizer and into a differential mobility analyzer (DMA, model 3081, TSI, Inc.) with stable voltage to create a monodisperse BC particles flow. A suite of high time resolution state-of-the-art aerosol instruments simultaneously measured a comprehensive set of BC properties throughout the BC aging process (Table S1). The particle diameter, mass, chemical composition, hygroscopicity and ability as cloud condensation nuclei (CCN) were measurement by a scanning mobility particle sizer (SMPS), a differential mobility analyzer–aerosol particle mass analyzer (DMA-APM) system, a high-resolution time-of-flight aerosol mass spectrometer (HR-ToF-AMS), a humidified tandem differential mobility analyzer (HTDMA) system, and a could condensation nuclei counter (CCNC), respectively. Detail information of the instruments is provided in the supplementary material and previous publications (DeCarlo et al., 2006; Khalizov et al., 2009). Specific measurement procedures in this study are discussed below.

DMA-APM measurement. The DMA-APM was used to measure the effective density of BC particles (Pagels et al., 2009). Before any DMA-APM measurement, a SMPS scan was made to obtain the size distribution of particles inside the chamber. The particle size distribution was then fitted with a lognormal Gaussian distribution to derive the peak diameter. During a DMA-APM measurement, the aerosol flow passed through DMA with a fixed voltage to select particles with a fixed diameter. The APM then measured the mass distribution of the selected particles with the same diameter, and the effective density of these particles was obtained by fitting the mass distribution with a normal Gaussian distribution.

DMA-CCN measurement. Similar to the density measurements, CCN activation was also measured on the basis of monodisperse particles with a peak diameter. A DMA with a fixed

160 voltage selected particles with a peak diameter. Both a CPC and a CCN counter were placed
161 in parallel after the DMA to simultaneously measure the total particle number concentration
162 (N_{cn}) as well as the activated number concentration (N_{ccn}) at a fixed supersaturation. The
163 activation fraction of the BC particles with peak diameter is calculated as:

164
$$f_{CCN} = \frac{N_{CN}}{N_{CCN}} \qquad (1)$$

165 Several gradients of supersaturation were set for the CCN counter, with each one being 6
166 min. This method yielded a steeper curve of the CCN activation rate, which was employed to
167 estimate the particle diameter with 50% activation fraction (D_{50}) and the kappa value.

168 Prior to each experiment, the QUALITY chamber was flushed by zero air for more than
169 40 hours to ensure a clean condition and covered with two layers of anti-UV cloth to shield it
170 from sunlight. In the beginning of each experiment, monodisperse BC particles were
171 introduced into the chamber. The injection of BC particles typically lasted for 1 to 2 hours.
172 During the injection period, zero air passed through the bottom chamber continually to
173 remove any possible remaining gaseous pollutant that were removed by the activated carbon.
174 After the injection, ambient air was pulled through the bottom chamber at a flow rate of about
175 50 L min^{-1} for at least half an hour in order to produce a quasi-ambient condition inside the
176 chamber. Finally, the anti-UV cloth was removed, and BC particles underwent aging inside
177 the reaction chamber. A charged zero air stream continuously passed through the space
178 between the two chamber layers to reduce particle wall loss. Various properties of BC
179 particles, including the particle diameter, mass, chemical composition, hygroscopicity, and
180 optical coefficients, were simultaneously measured by a suite of state-of-art aerosol
181 instruments in every 0.5 - 1 hour. Ambient particles and chamber particles were measured
182 alternately every 30 min. The aging experiments lasted for about 2-6 hours depending on the
183 initial BC concentrations and ambient conditions.

184 The BC aging experiments were conducted from August 18th to October 17th, 2013 at an
185 urban site (PKUERS) located on the campus of Peking University in the northwestern Beijing
186 (39.99°N, 116.31°E) (Hu et al., 2012).

3. Characterization and Validation of the QUALITY chamber

3.1 Wall loss of gases and aerosols

189 To evaluate the wall loss of both particles and gases in the QUALITY chamber, different
190 gaseous pollutants and particles were introduced into the chamber separately and the decay of
191 their concentration inside the chamber was measured by gas analyzers and SMPS,
192 respectively. All of the ports connected to the ambient air were closed to ensure an enclosed
193 system in the reaction chamber.

194 Particles with different chemical composition exhibited different wall loss rates.
195 Monodispersed BC particles with different diameters showed a small half-lifetime (τ) of
196 about 4-7 hours (Reed, 2010). Aerosol nucleation also occurred inside the chamber likely
197 from organic species (Zhao et al., 2009), which corresponded to a half time of about 3.5
198 hours (Fig. S3), because the nucleated particles inside the chamber was neutral with a slow
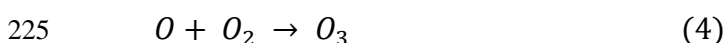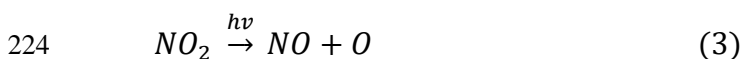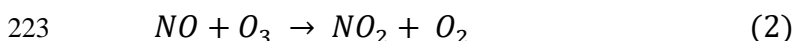
199 electrostatic loss to the wall.

200   Gas species had a longer residence time inside the chamber. Toluene and isoprene did
201 not show obvious wall loss during a two-day experiment (Reed, 2010). O_3, SO_2 and NO_x
202 decreased by 50% inside the chamber after more than 20 hours, suggesting slow loss. Since
203 the loss rate of these primary gaseous pollutants was much slower than the gas exchange rate
204 between the chamber, the loss of gases was replenished by the exchange with the flow
205 chamber.

206 **3.2 UV transmission**

207   The QUALITY chamber contained two layers of walls, an acrylic shell layer and a PFA
208 Teflon layer. Since the QUALITY chamber used sunlight as the photochemical origin, the
209 transmission spectra of the two-layer walls was of great important for the photochemical
210 reactions inside the reaction chamber.

211   The transmission efficiencies of each material were measured using an ultraviolet-visible
212 (UV-Vis) spectrophotometry (PerkinElmer Inc., model 552). As shown in Figure 2, the
213 Teflon film exhibited stable transmission efficiency of about 60% in the focused wavelength
214 range. The Acrylic shell, however, showed very low transmission efficiency when the
215 wavelength range was shorter than 270 nm, and high transmission efficiency (nearly 90%)
216 when the wavelength range was longer than 300 nm. In general, approximately 60% of the
217 UVA irradiation (315-400 nm range) and 50% of the UVB irradiation (280-315 nm range)
218 penetrated through the chamber walls, allowing photochemical processes to take place in the
219 upper reaction chamber.

220   A NO_2-photolysis experiment was also conducted to characterize the UV transmission of
221 QUALITY chamber. NO_2 was introduced inside the chamber at a clean and sunny day.
222 Reactions among NO_2, NO and O_3 will occur as the following equations:

223 $$NO + O_3 \rightarrow NO_2 + O_2 \qquad\qquad (2)$$

224 $$NO_2 \xrightarrow{hv} NO + O \qquad\qquad (3)$$

225 $$O + O_2 \rightarrow O_3 \qquad\qquad (4)$$

226   By simultaneously monitoring the concentrations of NO_2, NO and O_3 inside the chamber,
227 the photolysis constant of NO_2, $J(NO_2)$, inside the chamber was estimated. The photolysis
228 constant of NO_2 inside the chamber was on average 55% of that in the ambient air, in
229 agreement with the transmission spectra measurement, further confirming that the two-layer
230 chamber walls allowed 50% - 60% of solar irradiation in the UV range into the reaction
231 chamber.

232 **3.3 Gas concentrations in the reaction chamber**

233   To investigate the VOCs concentration inside the reaction chamber after the injection of
234 BC particles, both the chamber and ambient air were sampled with VOC canisters just before
235 the BC aging experiment started. These canisters were then analyzed by a gas
236 chromatography-mass spectrometer / flame ionization detector (GC-MS/FID, HP inc.) system

237 (Liu et al., 2008). The concentrations of VOCs containing 4 or more carbons are illustrated in
238 Figure 3. Slightly higher concentrations of several VOCs in the QUALITY chamber, e.g.,
239 n-butane, n-pentane, toluene, were observed compared with those in the ambient air, duo to
240 the co-injection of a small amount of VOCs together with BC particles into the chamber.
241 Nevertheless, the average increase of the VOC concentrations was only 16% or 0.1 ppb for
242 all focused VOCs species, with the largest increase of 35% or 0.36 ppb, suggesting the
243 insignificant influence of soot burner on VOCs concentrations and SOA formation in the
244 chamber.

245 Additional experiments were conducted to characterize the exchange time scale for gases
246 in the QUALITY chamber. The chamber was firstly cleaned and flushed with zero air for 40
247 hours. Ambient air was then pulled through the bottom chamber (Fig. 4), and the
248 concentrations of gaseous pollutants, including O_3, NO_x, CO, and SO_2, were measured
249 alternatively in the ambient air and in the upper chamber. In the beginning of the experiment
250 the concentrations of all gaseous species were lower than those in the ambient air. After
251 ambient air was pulled through the bottom chamber (labeled as the black dots in Fig. 4), the
252 concentrations of the gaseous pollutants in the reaction chamber increased sharply. For
253 example, the CO concentration inside the chamber was approximate 70% of that the ambient
254 concentration after 30-min mixing. The concentrations inside the chamber and ambient air
255 exhibited little difference after 1-hour mixing (Fig. 4c). Hence, the QUALITY chamber well
256 replicated the ambient gas concentrations. The gas exchange rate between the bottom and
257 reaction chambers was calculated to be approximately 0.06 min^{-1}.

3.4   Temperature and RH

259 The greenhouse effect for an outdoor chamber typically increases the temperature and
260 decreases the RH inside the chamber. For the QUALITY chamber, however, heat produced
261 by the greenhouse effect inside the chamber was effectively taken away as the ambient air
262 continuously passed through the bottom chamber and exchanged with air in the upper
263 chamber. As illustrated in Figure 5, there was little difference in temperature or RH inside
264 and outside the chamber, when the chamber experiments lasted for more than 1 hour,
265 suggesting that the QUALITY chamber effectively captured the ambient temperature and
266 RH.

3.5   Sulfuric acid production

268 Though gaseous pollutants such as SO_2, O_3, NO_x and VOCs penetrated into the reaction
269 chamber from the bottom chamber through the semi-permeable membrane, low volatile and
270 sticky gases, i.e., sulfuric acid, were unlikely to penetrate through the membrane (Fortner et
271 al., 2004). To characterize sulfuric acid production inside the chamber, we conducted a
272 special experiment by pulling ambient air into the bottom chamber, while injecting SO_2
273 directly into the reaction chamber. The experiment was conducted around noon on a clean
274 day when the O_3 concentration was around 50 ppb. A custom-made atmospheric pressure-ion
275 drift chemical ionization mass spectrometry (AP-ID-CIMS) (Fortner et al., 2004; Zheng et al.,
276 2010) was used to directly measure the concentration of gaseous sulfuric acid. Fig. 6 shows a
277 good correlation between SO_2 and gaseous H_2SO_4 inside the chamber, suggesting that the
278 QUALITY chamber well simulated the formation of low volatile gaseous species and hence

279 the photochemical processes.

4. BC evolution in the QUALITY chamber

281 Time series of the ambient PM, gas, and meteorology parameters of ambient air during
282 chamber experiment period are illustrated in Figure 7. Except for the last experiment
283 conducted on October 17th, all experiments were conducted between August 18th, 2013 and
284 September 21st, 2013. During this period in Beijing, strong photochemical reactions and
285 frequent heavy pollution events occurred (Huang et al., 2010; Zhao et al., 2013). Temperature
286 and RH during this period (August 18th to September 21st) varied from 24°C to 38°C and
287 from 20 % to 90 %, respectively. The average concentration of $PM_{2.5}$, SO_2 and NO_x were 60
288 $\pm$ 45 μg m^{-3}, 3.2 $\pm$ 2.6 ppb and 33.9 $\pm$ 20.9 ppb, respectively.

289 The red shaded areas in Figure 7 represent the period of the nine chamber experiments.
290 In general, chamber experiments were conducted in the afternoon of relatively clean and
291 sunny days, when strong solar radiation led to fast photochemical reactions. There were two
292 experiments conducted under polluted days, e.g., the experiments on October 22rd and
293 September 11th. Table 1 summaries the conditions of the experiments. Totally, 10 BC aging
294 experiments were conducted, including four experiments using BC particles with initial
295 mobility diameter of 100 nm, three experiments using 150 nm particles, and three using 220
296 nm BC particles. The average concentrations of $PM_{2.5}$ and NO_x over each chamber
297 experiment were only 9 to 69 μg m^{-3} and 9 to 41 ppb, respectively. The concentrations of
298 VOCs, such as toluene and m/p-xylene were relatively low during most of the experiments
299 compared with severe pollution episodes in Beijing (Guo et al., 2014). $J(O^1D)$ and O_3
300 exhibited higher values during the chamber experiments. The average $J(O^1D)$ values and O_3
301 concentrations ranged from 3.2×10^{-6} s^{-1} to 21.1×10^{-6} s^{-1} and 26 to 92 ppb, respectively.

4.1 BC growth

303 To quantify the growth of BC particles, several parameters were used to describe the
304 properties of BC particle, including the effective density, mobility diameter and mass
305 equivalent diameter. Material density (ρ_m) is the average density of the solid and liquid
306 material in the particle. Assuming that the volume of the species coexisting in an individual
307 particle does not change upon mixing, the density of an internally mixed particle is calculated
308 using the material densities and mass concentrations of particulate constituents (DeCarlo et
309 al., 2004; Pagels et al., 2009),

$$\rho_m = \frac{\sum_{species} m_i}{\sum_{species} V_i} = \frac{\sum_{species} m_i}{\sum_{species} \frac{m_i}{\rho_i}} = \frac{\sum_{species} MC_i}{\sum_{species} \frac{MC_i}{\rho_i}} \qquad (5)$$

311 where ρ_i is the material density of species i, V_i is its volume, m_i is its mass, and MC_i is its
312 mass concentration. This approach is based on the assumption that there is no void space
313 enclosed within the particle envelope. Hence, the material density is larger than the true
314 particle density with internal voids in particles. In this study, ρ_m is calculated from the
315 chemical composition of coating materials measured by AMS. A value of 1.35 for the
316 material density of SOA formed during chamber experiment was obtained by directly
317 measuring the density of newly form particles inside the chamber via DMA-APM system.

318   Effective density (ρ_{eff}) is defined as the ratio of the measured particle mass (m_p) to the
319 particle volume calculated assuming a spherical particle with a diameter equal to the
320 measured mobility diameter (D_m) (DeCarlo et al., 2004; Pagels et al., 2009; Xue et al.,
321 2009b):

322
$$\rho_{eff} = \frac{6m_p}{\pi D_m^3} \quad\quad (6)$$

323   In this study, m_p of BC particles was measured by the APM and mobility diameter (D_m)
324 was measured by the DMA. The effective density reflects the information on both particle
325 density and shape. If particles are spherical in the absence of internal void, the effective
326 density equals the material density. If particles are non-spherical, the calculated volume and
327 volume concentration are larger than the true values, and the effective density is less than true
328 particle and the material density.

329   Figure 8 exhibits the change of particle density and diameter in three typical BC aging
330 experiments using BC particles with the initial diameter of 100 nm, 150 nm, and 220 nm
331 (experiment #4, #5, and # 9 in Table 1, respectively). The average $PM_{2.5}$ concentrations in
332 these experiments were 40, 27, and 12 μg m^{-3}, respectively, suggesting relatively clean
333 conditions during the experiments. In all three experiments, aging of BC particles occurred
334 between 13:00-14:00 and 17:00 in the afternoon. The highest $J(O^1D)$ value varied from 1.7 to
335 2.4×10^{-5} s^{-1} and decreased generally over the experiment period. Average O_3 concentrations
336 during the three experiments were 68, 83 and 54 ppb, respectively, indicating strong
337 oxidation during the experiment periods.

338   For three initial D_m of 100 nm, 150 nm, and 200 nm, the ranges of effective density of
339 fresh BC particles in each experiment were 0.43-0.50 g cm^{-3}, 0.34-0.34 g cm^{-3}, and 0.24-0.32
340 g cm^{-3}, respectively, indicating highly fractal BC aggregates (Zhang et al., 2008). The small
341 variation for particles with the same D_m also demonstrates the consistency of fresh BC
342 morphology in different experiments. After aging of 1 hour, ρ_{eff} of BC particles in the three
343 experiments increased to approximately 1.2 g cm^{-3}, suggesting that formation of the
344 secondary components changed the morphology from chain-like BC particles into a more
345 compact shape (Zhang et al., 2008; Peng et al., 2016). The morphology change was further
346 confirmed by a decrease of D_m, particularly for larger BC particles that were more fractal
347 than smaller BC particles.

348   As the D_m is largely influenced by the particle morphology, we utilized the parameter of
349 mass equivalent diameter (D_{me}) to describe the growth of particles. Based on the mobility
350 diameter (D_m), material density (ρ_m) and effective density (ρ_{eff}), the D_{me} is calculated
351 assuming that particles are compact and with a spherical morphology (DeCarlo et al., 2004):

352
$$D_{me} = \sqrt[3]{\frac{\rho_{eff}}{\rho_m}} D_m \quad\quad (7)$$

353 The change in the mass equivalent diameter (ΔD_{me}) during BC aging is defined as the total
354 coating thickness, and the ratio of the total coating thickness to the initial mass equivalent
355 diameter ($\Delta D_{me}/D_{me,0}$) is defined as the coating fraction.

The initial D_{me} of fresh BC particles with initial D_m of 100, 150 and 220 nm were 61, 84 and 114 nm, respectively. In contrast to the mobility diameter, D_{me} increased continuously during the entire experiment. After 3-4 hours, D_{me} in the three experiments increased to 133, 169 and 197 nm, respectively (Fig. 8), with the average growth rates of 19, 29 and 31 nm h^{-1}. Higher growth rates in D_{me} occurred around noontime, when the $J(O^1D)$ value was higher and the photochemical reaction was stronger. On the other hand, much less growth rate was observed during late afternoon or with cloud coverage (As shown in Fig. 8c at 15:00), indicating that the growth was driven by photochemical reactions.

The increases of the particle density and diameter in all the experiments are summarized in Table 2. Fast aging of BC particles occurred in all experiments. The total growth of D_{me} ranged from 40 nm to 152 nm within 3-6 hours, with an average growth of 73 nm. The average growth rate was 26 ± 11 nm h^{-1}, demonstrating large secondary production under the ambient conditions in Beijing. The largest growth rate (ΔD_{me} = 152 nm) was observed in experiment #8, when solar irradiation was the strongest among all experiments (Table 2).

Correlation analysis was made between the average growth rate of BC particles ($\Delta D_{me}/\Delta t$) with O_3, $PM_{2.5}$, $J(O^1D)$, and temperature during the different experiments (Fig. S4). The growth rate of BC particles exhibits no correlation with O_3 concentration (R^2=0.00), weak negative correlation with $PM_{2.5}$ concentration (R^2 = 0.25), and strong positive correlations with $J(O^1D)$ (R^2 = 0.80) and temperature (R^2 = 0.67), indicating the importance of photochemical production on the BC coating materials.

4.2   Chemical composition of coating materials

Particle composition measurements by AMS during chamber experiments reveal a majority of coating materials (above 90%) as SOA (Fig. 8). The concentration of SOA inside the chamber reached up to 9 μg m^{-3} in several experiments, suggesting fast formation of SOA via gas phase oxidation of VOCs. The SOA formation in Beijing is likely attributed to a large amount of anthropogenic aromatic VOCs (Peng et al., 2017).

The elemental compositions of OA inside the chamber, i.e., the oxygen to carbon (O/C) ratio and the hydrogen to carbon (H/C) ratio, were calculated based on the updated ambient calibrations (He et al., 2011; Canagaratna et al., 2015). The H/C and O/C ratios of organics for coating on BC particles exhibit notable trends during the aging process. Figure 9A shows an example of the evolution of H/C and O/C ratios in experiment #8. The data were corrected for the CO_2 concentration in the chamber, which were introduced into the chamber with BC particles and influenced the abundance of m/z = 28 and 44 in the AMS mass spectra. The H/C ratio decreased from 1.73 to 1.45 over six hours. Accordingly, the O/C ratio increased from 0.32 to 0.50 during the same time, revealing that further oxidation of SOA occurred in the latter part of the experiment. The lower final O/C ratio in the chamber experiment (0.5) than that under the ambient conditions (Hu et al., 2016) implies that there is oxidation on a longer timescale or by the aqueous pathway for the formation of highly oxidized SOA in the ambient air (Zhang et al., 2015).

Furthermore, the mass spectra of OA inside the chamber shows strong correlation with the less-oxidized oxygenated organic aerosols (LO-OOA) derived from field measurements

397   in Beijing (Hu et al., 2016), which likely arose from oxidation of aromatic VOCs emitted
398   from vehicles (Peng et a., 2017). The correlation coefficient (R^2) initially was 0.88 and raised
399   to 0.99 sharply (Fig. 9B), indicating that the chamber well simulated the formation of
400   LO-OOA.

401   In our study, the secondary inorganic aerosols, i.e., sulfate, nitrate and ammonium, only
402   accounted for less than 10% of the coating materials on BC particles. This is consistent with
403   the previous studies showing that the concentration of organics is much larger than those of
404   sulfate and nitrate during the early stage of haze development in Beijing (Guo et al., 2014).
405   The low observed sulfate concentration in this study suggests that the gas phase formation of
406   sulfuric acid was unimportant under our experimental conditions. On the other hand, it has
407   been shown that the aqueous-phase reactions represent the dominate pathway for sulfate
408   formation in Beijing (Guo et al., 2010; Wang et al., 2016).

409   NO_2 has a higher reaction coefficient with the OH radical ($8 \times 10^{-12}\,cm^3$ molecule^{-1} s^{-1})
410   than SO_2 (Zhang et al., 2015). Nitrate acid formed in the gas phase is transformed into nitrate
411   salts by the reaction with ammonia in the equilibrium process:

$$HNO_3(g) + NH_3(g) \leftrightarrow NH_4NO_3(s) \qquad (8)$$

413   The equilibrium of this reaction is highly depended on ambient temperature and RH (Zheng
414   et al., 2008). In this study, chamber experiments were conducted in the afternoon with high
415   temperature and low RH (Table 1), which shifted the thermodynamic equilibrium to the gas
416   phase.

4.3   Hygroscopicity evolution

HTDMA measurement

419   The hygroscopic growth factors (HGF) of particles in each experiment were
420   continuously measured by the HTDMA system and corrected for the reference "dry"
421   diameters,

$$HGF = \frac{D_{wet,t}/D_{m,t}}{D_{dry,0}/D_{m,0}} \qquad (9)$$

423   where D_m is the mobility diameter of fresh or coated particles at dry condition, D_{dry} is the
424   mobility diameter of particles after experiencing a low humidity (below 30%) cycle in
425   HTDMA, and D_{wet} is the mobility diameter of particles after experiencing a high humidity
426   cycle (87%) in HTDMA.

427   Figure 10 shows the hygroscopicity variation of BC particles with the initial mobility
428   diameter ($D_{m,0}$) of 100 nm and 150 nm. The measured HGF of 0.999 - 1.004 for fresh BC
429   particles suggests high hydrophobicity, consistent with the previous studies (Khalizov et al.,
430   2009;Weingartner et al., 1997). After exposed to sunlight and ambient gaseous pollutants for
431   several hours, the HGF of these BC particles increased to 1.02-1.08 at the end of each
432   experiment. The HGF value varied with the total growth (ΔD_{me}) of BC particles, but was
433   constant at the same ΔD_{me} for different experiments (Fig. 10). The final HGF values shown in

434 Figure 10 (1.02-1.08) were much lower than those in previous laboratory studies (Khalizov et
435 al., 2009;Tritscher et al., 2011) but similar to the low hygroscopic fraction in field
436 observations (Swietlicki et al., 2008), even for growth of particle size up to 90 nm in our
437 experiments.

438 The HGF is affected by many factors, e.g., the particle chemical composition and
439 morphology as well as RH (Qiu et al., 2012). The hygroscopicity of BC particles coated with
440 inorganic components, i.e., sulfuric acid (Khalizov et al., 2009), is significantly higher than
441 that coated by organic compounds (Tritscher et al., 2011). In this study, the major component
442 of the coating substance was LO-OOA with a O/C ratio about 0.5. The low oxygen content of
443 SOA coated on BC particles explains the low hygroscopicity (Jimenez et al., 2009),
444 indicating that coating of BC particles during the early stage haze development in Beijing
445 does not considerably increase the particle hygroscopicity.

446 The morphology of BC particles directly affects the HGF. As illustrated in Figure 11,
447 when the ΔD_{me} was 18 nm and 22 nm for 100 nm and 150 nm BC particles, respectively, the
448 HGF decreased slightly to about 0.99, suggesting that a thin layer of coatings on BC particles
449 decreased the particle diameter, even though a certain amount of water absorbed by BC
450 particles increased the particle mass. The surface tension of the water layer produced an
451 inward force on the "chain-like" branches of BC particles, leading to particle reconstruction,
452 and a more compact morphology. Such change was also identified in laboratory studies
453 (Weingartner et al., 1997; Tritscher et al., 2011; Qiu et al., 2012). In this study, the BC
454 particles became spherical when ΔD_{me} was 30 nm and 40 nm for particles with initial D_m of
455 100 nm and 150 nm, respectively (Peng et al., 2016). Therefore, when ΔD_{me} was large, the
456 HGF value was not influenced by reconstruction.

457 ### *CCN measurements and κ closure*

458 The CCN activation faction (f_{CCN}) of BC particles at different supersaturation during two
459 typical experiments is illustrated in Figure 11. Fresh BC particles were not activated even at
460 very high supersaturation conditions (0.7%). With aging, f_{CCN} rapidly raised to nearly 100%
461 at high supersaturation (0.7% for experiment #4 and 0.6% for experiment #6). After several
462 hours, BC particles became CCN at lower supersaturation. The f_{CCN} at 0.4 supersaturation
463 (Fig. 11a in experiment #4) and 0.3 supersaturation (Fig. 11b in experiment #6) exceeded 50%
464 before the end of these two experiments, suggesting that aging increases the ability of BC
465 particles to become CCN (Wittbom et al., 2014) and a large amount of coatings results in
466 activation at lower supersaturation.

467 To further investigate the hygroscopicity of BC particles and combine the measurements
468 using HTDMA and CCN, we evaluated the hygroscopicity parameter, kappa (κ) (Petters and
469 Kreidenweis, 2007). The approximate relationship between the dry particle mass equivalent
470 diameter (D_{me}), the critical saturation ratio (Sc) and the apparent κ value of particles is
471 describe as:

472 $$\kappa = \frac{4A^3}{27D_{me}\ln^2 S_c} \qquad (10)$$

473 where A is a parameter that includes several features of the solvent,

474    $$A = \frac{4\sigma_{s/a} M_w}{RT\rho_w} \qquad (11)$$

475   M_w is the molecular weight of water, ρ_w is the density of water, $\sigma_{s/a}$ is the surface tension of
476   the solution/air interface, R is the universal gas constant, and T is temperature.

477   In addition to the supersaturated condition, the κ theory also adopts the form for the
478   subsaturated condition, using the HGF from HTDMA measurement and RH:

479    $$\frac{RH}{exp\left(\frac{A}{D_{wet}}\right)} = \frac{HGF^3 - 1}{HGF^3 - (1-\kappa)} \qquad (12)$$

480   where D_{wet} is the wet diameter of particles.

481   The apparent κ values of BC particles calculated by HTDMA (κ_HTDMA) and CCN
482   (κ_CCN) are shown in Figure 11. The κ of fresh BC particles was near zero. With aging,
483   SOA coated on BC particles increased the κ_HTDMA and κ_CCN to approximately 0.04,
484   although the κ_HTDMA and κ_CCN exhibited difference features. A slightly higher κ_CCN
485   than κ_HTDMA at the beginning of aging was identified, attributed to reconstruction of BC
486   particles after humidified and underestimation of HGF and thus the κ_HTDMA value. Such a
487   difference between κ_CCN and κ_HTDMA was also observed in previous studies (Tritscher
488   et al., 2011; Martin et al., 2013). Nevertheless, the apparent κ values from two both methods
489   were comparable at the end of both experiments.

490   Assuming that a simple mixing rule is applicable to coated BC particles, the κ for
491   coating materials can be calculated based on the volume fraction of BC and SOA:

492    $$\kappa = \sum_i \varepsilon_i \kappa_i \qquad (13)$$

493   where ε_i represents the volume fraction of species i. Since the SOA formed inside the
494   chamber was not highly hygroscopic, some of the SOA components might not be able to
495   solve in water droplets (Petters and Kreidenweis, 2008), leading to the underestimation of the
496   κ values of the coating materials in this study.

497   The κ values of the coating materials were 0.04 at the end of our experiments for both
498   CCN and HTDMA method, much lower than that of ambient aerosols in Beijing (Gunthe et
499   al., 2011; Wu et al., 2016) and those of SOA in previous chamber studies (Jimenez et al.,
500   2009; Tritscher et al., 2011; Martin et al., 2013). As discussed above, the coating substances
501   on BC particles were mainly SOA formed from photochemical oxidation. The κ of SOA
502   depends on the oxidation degree, which is correlated to the O/C ratio (Jimenez et al., 2009;
503   Massoli et al. 2010). The O/C ratio of the coating SOA was 0.5 in our experiment,
504   corresponding to the O/C ratio of approximately 0.4 in Jimenez et al. (2009) and Massoli et
505   al. (2010) duo the utilize of updated AMS calibration method in this study. The κ value of
506   coating materials here is in general slightly lower than those of SOA with similar oxidation
507   degree (O/C ratio) formed from different VOCs precursors (Jimenez et al., 2009; Massoli et
508   al. 2010). As motion above, the κ values of the coating materials might be underestimated
509   duo to the ignore of solubility of the SOA products. Also, our experiments represent the aging

of BC under typical urban condition, where variety of anthropogenic VOCs, i.e., toluene, xylene, TMB and small molecular PAHs, contribute significantly to the SOA formation. Some products of these VOC precursors may exhibit low hygroscopicity.

5 Conclusions

In this paper, we present measurements of aging and hygroscopicity of BC particles in Beijing using the QUALITY chamber. The unique two sub-chamber design facilitates the evaluation of aging of BC particles under ambient conditions, by mimicking the ambient gaseous concentrations without the presence of ambient aerosols. High UV transmission efficiency (50-60%) and negligible wall loss of primary gaseous pollutants are shown for the chamber performance. The validation experiments demonstrate little differences in the primary gas concentrations, temperature, and RH between the chamber and the atmosphere, suggesting that the chamber captures the evolution of ambient conditions. In addition, our results show sulfuric acid production correlated with SO_2, indicating that the chamber well simulates photochemical-driven formation of low volatile gaseous species by the hydroxyl radical.

BC aging experiments were performed using the QUALITY chamber in Beijing. Fast growth of BC particles (on average 26 ± 11 nm h^{-1}) was observed, and SOA was identified as the dominate component of the coating materials on BC particles, while inorganic species, such as sulfate and nitrate, were unimportant under our experimental condition and timescale.

The HGF of BC particles exhibited a very low value (1.02-1.08) after several hours aging. A slight decrease of HGF with a thin coating layer indicated reconstruction of BC particles after humidified. Also, a very low kappa value (0.035) for BC particles at both subsaturation and supersaturation conditions were found, with HTDMA and CCN measurements. Hence, our results indicate that initial photochemical aging of BC particles does not appreciably alter the particle hygroscopicity in Beijing.

References

Bond, T. C., Doherty, S. J., Fahey, D. W., Forster, P. M., Berntsen, T., DeAngelo, B. J., Flanner, M. G., Ghan, S., Kärcher, B., Koch, D., Kinne, S., Kondo, Y., Quinn, P. K., Sarofim, M. C., Schultz, M. G., Schulz, M., Venkataraman, C., Zhang, H., Zhang, S., Bellouin, N., Guttikunda, S. K., Hopke, P. K., Jacobson, M. Z., Kaiser, J. W., Klimont, Z., Lohmann, U., Schwarz, J. P., Shindell, D., Storelvmo, T., Warren, S. G., and Zender, C. S.: Bounding the role of black carbon in the climate system: A scientific assessment, Journal of Geophysical Research: Atmospheres, 118, 5380-5552, 10.1002/jgrd.50171, 2013.

Canagaratna, M. R., Jimenez, J. L., Kroll, J. H., Chen, Q., Kessler, S. H., Massoli, P., Hildebrandt Ruiz, L., Fortner, E., Williams, L. R., Wilson, K. R., Surratt, J. D., Donahue, N. M., Jayne, J. T., and Worsnop, D. R.: Elemental ratio measurements of organic compounds using aerosol mass spectrometry: characterization, improved calibration, and implications, Atmos. Chem. Phys., 15, 253-272, doi:10.5194/acp-15-253-2015, 2015.

Claeys, M.: Formation of Secondary Organic Aerosols Through Photooxidation of Isoprene, Science, 303, 1173-1176, doi:10.1126/science.1092805, 2004.

DeCarlo, P. F., Slowik, J. G., Worsnop, D. R., Davidovits, P., and Jimenez, J. L.: Particle Morphology and Density Characterization by Combined Mobility and Aerodynamic Diameter Measurements. Part 1: Theory, Aerosol Sci. Tech., 38, 1185-1205, 10.1080/027868290903907, 2004.

DeCarlo, P. F., Kimmel, J. R., Trimborn, A., Northway, M. J., Jayne, J. T., Aiken, A. C., Gonin, M., Fuhrer, K., Horvath, T., Docherty, K. S., Worsnop, D. R., and Jimenez, J. L.: Field-deployable, high-resolution, time-of-flight aerosol mass spectrometer, Anal. Chem., 78, 8281-8289, doi:10.1021/ac061249n, 2006.

DeCarlo, P. F., Ulbrich, I. M., Crounse, J., de Foy, B., Dunlea, E. J., Aiken, A. C., Knapp, D., Weinheimer, A. J., Campos, T., Wennberg, P. O., and Jimenez, J. L.: Investigation of the sources and processing of organic aerosol over the Central Mexican Plateau from aircraft measurements during MILAGRO, Atmos. Chem. Phys., 10, 5257-5280, doi:10.5194/acp-10-5257-2010, 2010.

Ervens, B., Turpin, B. J., and Weber, R. J.: Secondary organic aerosol formation in cloud droplets and aqueous particles (aqSOA): a review of laboratory, field and model studies, Atmos. Chem. Phys., 11, 11069-11102, doi:10.5194/acp-11-11069-2011, 2011.

Fortner, E. C., Zhao, J., and Zhang, R. Y.: Development of ion drift-chemical ionization mass spectrometry, Anal. Chem., 76, 5436-5440, doi:10.1021/ac0493222, 2004.

Gunthe, S. S., Rose, D., Su, H., Garland, R. M., Achtert, P., Nowak, A., Wiedensohler, A., Kuwata, M., Takegawa, N., Kondo, Y., Hu, M., Shao, M., Zhu, T., Andreae, M. O., and Pöschl, U.: Cloud condensation nuclei (CCN) from fresh and aged air pollution in the megacity region of Beijing, Atmos. Chem. Phys., 11, 11023-11039, doi:10.5194/acp-11-11023-2011, 2011.

Guo, S., Hu, M., Lin, Y., Gomez-Hernandez, M., Zamora, M. L., Peng, J. F., Collins, D. R., and Zhang, R. Y.: OH-Initiated Oxidation of m-Xylene on Black Carbon Aging, Environ. Sci. Technol., 50, 8605-8612, doi:10.1021/acs.est.6b01272, 2016.

Guo, S., Hu, M., Wang, Z. B., Slanina, J., and Zhao, Y. L.: Size-resolved aerosol water-soluble ionic compositions in the summer of Beijing: implication of regional secondary formation, Atmos. Chem. Phys., 10, 947-959, 2010.

Guo, S., Hu, M., Zamora, M. L., Peng, J., Shang, D., Zheng, J., Du, Z., Wu, Z., Shao, M., Zeng, L., Molina, M. J., and Zhang, R.: Elucidating severe urban haze formation in China, P. Natl. Acad. Sci. USA, 111, 17373-17378, doi:10.1073/pnas.1419604111, 2014.

He, L.-Y., X.-F. Huang, L. Xue, M. Hu, Y. Lin, J. Zheng, R. Zhang, and Y.-H. Zhang: Submicron aerosol analysis and organic source apportionment in an urban atmosphere in Pearl River Delta of China using high-resolution aerosol mass spectrometry, J. Geophys. Res. 116, D12304, doi:10.1029/2010JD014566, 2011.

Hu, M., Peng, J., Sun, K., Yue, D., Guo, S., Wiedensohler, A., and Wu, Z.: Estimation of Size-Resolved Ambient Particle Density Based on the Measurement of Aerosol Number, Mass, and Chemical Size Distributions in the Winter in Beijing, Environ. Sci. Technol., 46, 9941-9947, doi:10.1021/es204073t, 2012.

Hu, W., Hu, M., Hu, W., Jimenez, J. L., Yuan, B., Chen, W., Wang, M., Wu, Y., Chen, C., Wang, Z., Peng, J., Zeng, L., and Shao, M.: Chemical composition, sources and aging process of sub-micron aerosols in Beijing: contrast between summer and winter, J. Geophys. Res.- Atmos., 121, 1955-1977 doi:10.1002/2015jd024020, 2016.

Huang, X. F., He, L. Y., Hu, M., Canagaratna, M. R., Sun, Y., Zhang, Q., Zhu, T., Xue, L., Zeng, L. W., Liu, X. G., Zhang, Y. H., Jayne, J. T., Ng, N. L., and Worsnop, D. R.: Highly time-resolved chemical characterization of atmospheric submicron particles during 2008 Beijing Olympic Games using an Aerodyne High-Resolution Aerosol Mass Spectrometer, Atmos. Chem. Phys., 10, 8933-8945, doi:10.5194/acp-10-8933-2010, 2010.

Intergovernmental Panel on Climate Change (IPCC), Climate Change 2013: The Physical Science Basis, Cambridge Univ. Press, Cambridge, UK, 2013.

Jacobson, M. Z.: Strong radiative heating due to the mixing state of black carbon in atmospheric aerosols, Nature, 409, 695-697, doi:10.1038/35055518, 2001.

Jimenez, J. L., Canagaratna, M. R., Donahue, N. M., Prevot, A. S. H., Zhang, Q., Kroll, J. H., DeCarlo, P. F., Allan, J. D., Coe, H., Ng, N. L., Aiken, A. C., Docherty, K. S., Ulbrich, I. M., Grieshop, A. P., Robinson, A. L., Duplissy, J., Smith, J. D., Wilson, K. R., Lanz, V. A., Hueglin, C., Sun, Y. L., Tian, J., Laaksonen, A., Raatikainen, T., Rautiainen, J., Vaattovaara, P., Ehn, M., Kulmala, M., Tomlinson, J. M., Collins, D. R., Cubison, M. J., Dunlea, J., Huffman, J. A., Onasch, T. B., Alfarra, M. R., Williams, P. I., Bower, K., Kondo, Y., Schneider, J., Drewnick, F., Borrmann, S., Weimer, S., Demerjian, K., Salcedo, D., Cottrell, L., Griffin, R., Takami, A., Miyoshi, T., Hatakeyama, S., Shimono, A., Sun, J. Y., Zhang, Y. M., Dzepina, K., Kimmel, J. R., Sueper, D., Jayne, J. T., Herndon, S. C., Trimborn, A. M., Williams, L. R., Wood, E. C., Middlebrook, A. M., Kolb, C. E., Baltensperger, U., and Worsnop, D. R.: Evolution of Organic Aerosols in the Atmosphere, Science, 326, 1525-1529, doi:10.1126/science.1180353, 2009.

Kalberer, M.: Identification of Polymers as Major Components of Atmospheric Organic Aerosols, Science, 303, 1659-1662, doi:10.1126/science.1092185, 2004.

Khalizov, A. F., Xue, H., and Zhang, R.: Enhanced light absorption and scattering by carbon soot aerosols internally mixed with sulfuric acid, J. Phys. Chem., 113, 1066–1074, doi:10.1021/jp807531n, 2009.

Khalizov, A. F., Zhang, R., Zhang, D., Xue, H., Pagels, J., and McMurry, P. H.: Formation of highly hygroscopic soot aerosols upon internal mixing with sulfuric acid vapor, J. Geophys. Res., 114, doi:10.1029/2008jd010595, 2009.

635 Khalizov, A. F., Lin, Y., Qiu, C., Guo, S., Collins, D., and Zhang, R.: Role of OH-Initiated
636   Oxidation of Isoprene in Aging of Combustion Soot, Environ. Sci. Technol., 47,
637   2254-2263, doi:10.1021/es3045339, 2013.
638 Kuwata, M., Kondo, Y., Mochida, M., Takegawa, N., and Kawamura, K.: Dependence of
639   CCN activity of less volatile particles on the amount of coating observed in Tokyo, J.
640   Geophys. Res., 112, doi:10.1029/2006jd007758, 2007.
641 Liu, S., Aiken, A. C., Gorkowski, K., Dubey, M. K., Cappa, C. D., Williams, L. R., Herndon,
642   S. C., Massoli, P., Fortner, E. C., Chhabra, P. S., Brooks, W. A., Onasch, T. B., Jayne, J. T.,
643   Worsnop, D. R., China, S., Sharma, N., Mazzoleni, C., Xu, L., Ng, N. L., Liu, D., Allan, J.
644   D., Lee, J. D., Fleming, Z. L., Mohr, C., Zotter, P., Szidat, S., and Prevot, A. S. H.:
645   Enhanced light absorption by mixed source black and brown carbon particles in UK
646   winter, Nat. Commun., 6, Artn 8435, doi:10.1038/Ncomms9435, 2015.
647 Liu, Y., Shao, M., Fu, L. L., Lu, S. H., Zeng, L. M., and Tang, D. G.: Source profiles of
648   volatile organic compounds (VOCs) measured in China: Part I, Atmospheric Environment,
649   42, 6247-6260, doi:10.1016/j.atmosenv.2008.01.070, 2008.
650 Ma, Y., Brooks, S. D., Vidaurre, G., Khalizov, A. F., Wang, L., and Zhang, R.: Rapid
651   modification of cloud-nucleating ability of aerosols by biogenic emissions, Geophys. Res.
652   Lett., 40, 6293-6297, doi:10.1002/2013gl057895, 2013.
653 Martin, M., Tritscher, T., Jurán.yi, Z., Heringa, M. F., Sierau, B., Weingartner, E., Chirico, R.,
654   Gysel, M., Prévôt, A. S. H., Baltensperger, U., and Lohmann, U.: Hygroscopic properties
655   of fresh and aged wood burning particles, J. Aerosol Sci., 56, 15-29,
656   doi:10.1016/j.jaerosci.2012.08.006, 2013.
657 Massoli, P., Lambe, A. T., Ahern, A. T., Williams, L. R., Ehn, M., Mikkilä, J., Canagaratna, M.
658   R., Brune, W. H., Onasch, T. B., Jayne, J. T., Petäjä, T., Kulmala, M., Laaksonen, A., Kolb,
659   C. E., Davidovits, P., Worsnop, D. R.: Relationship between aerosol oxidation level and
660   hygroscopic properties of laboratory generated secondary organic aerosol (SOA) particles.
661   Geophys. Res. Lett., 37, L24801, doi:10.1029/2010GL045258, 2010.Moffet, R. C., and
662   Prather, K. A.: In-situ measurements of the mixing state and optical properties of soot
663   with implications for radiative forcing estimates, P. Natl. Acad. Sci. USA, 106,
664   11872-11877, doi:10.1073/pnas.0900040106, 2009.
665 Pagels, J., McMurry, P.H., Khalizov, A.F., and Zhang, R.: Processing of soot by controlled
666   sulphuric acid and water condensation—Mass and mobility relationship, Aerosol Sci.
667   Tech. 43, 629–640, 2009.
668 Peng, J., Hu, M., Du, Z., Wang, Y., Zheng, J., Zhang, W., Yang, Y., Qin, Y., Zheng, R., Xiao,
669   Y., Wu, Y., Lu, S., Wu, Z., Guo, S., Mao, H., and Shuai, S.: Gasoline aromatic: a critical
670   determinant of urban secondary organic aerosol formation, Atmos. Chem. Phys. Discuss.,
671   doi:10.5194/acp-2017-254, 2017.
672 Peng, J. F., Hu, M., Guo, S., Du, Z. F., Zheng, J., Shang, D. J., Zamora, M. L., Zeng, L. M.,
673   Shao, M., Wu, Y. S., Zheng, J., Wang, Y., Glen, C. R., Collins, D. R., Molina, M. J., and
674   Zhang, R. Y.: Markedly enhanced absorption and direct radiative forcing of black carbon
675   under polluted urban environments, P. Natl. Acad. Sci. USA, 113, 4266-4271,
676   doi:10.1073/pnas.1602310113, 2016.
677 Peng, J. F., Hu, M., Wang, Z. B., Huang, X. F., Kumar, P., Wu, Z. J., Guo, S., Yue, D. L.,
678   Shang, D. J., Zheng, Z., and He, L. Y.: Submicron aerosols at thirteen diversified sites in

China: size distribution, new particle formation and corresponding contribution to cloud condensation nuclei production, Atmos. Chem. Phys., 14, 10249-10265, doi:10.5194/acp-14-10249-2014, 2014.

Petters, M. D., and Kreidenweis, S. M.: A single parameter representation of hygroscopic growth and cloud condensation nucleus activity, Atmos. Chem. Phys., 7, 1961-1971, 2007.

Petters, M. D., and Kreidenweis, S. M.: A single parameter representation of hygroscopic growth and cloud condensation nucleus activity—Part 2: Including solubility, Atmos. Chem. Phys., 8, 6273– 6279, 2008.

Qiu, C., Khalizov, A. F., and Zhang, R. Y.: Soot Aging from OH-Initiated Oxidation of Toluene, Environ. Sci. Technol., 46, 9464-9472, doi:10.1021/Es301883y, 2012.

Qiu, C., and Zhang, R.: Multiphase chemistry of atmospheric amines, Phys. Chem. Chem. Phys. 15, doi:10.1039/C3CP43446J, 5738-5752, 2013.

Reed, R. C.: Observations of secondary organic aerosol production and soot aging under atmospheric conditions using a novel new environmental aerosol chamber, PhD dissertation, Texas A&M Univ, College Station, TX,. 2010.

Ruehl, C. R., Davies, J. F., and Wilson, K. R.: An interfacial mechanism for cloud droplet formation on organic aerosols, Science, 351, 1447-1450, doi:10.1126/science.aad4889, 2016.

Saathoff, H., Naumann, K. H., Schnaiter, M., Schöck, W., Möhler, O., Schurath, U., Weingartner, E., Gysel, M., and Baltensperger, U.: Coating of soot and (NH4)2SO4 particles by ozonolysis products of α-pinene, J. Aerosol Sci., 34, 1297-1321, doi:10.1016/s0021-8502(03)00364-1, 2003.

Santoro, R. J., Semerjian, H. G., and Dobbins, R. A.: Soot Particle Measurements in Diffusion Flames, Combust. Flame, 51, 203-218, 1983.

Swietlicki, E., Hansson, H. C., HÄMeri, K., Svenningsson, B., Massling, A., McFiggans, G., McMurry, P. H., PetÄJÄ, T., Tunved, P., Gysel, M., Topping, D., Weingartner, E., Baltensperger, U., Rissler, J., Wiedensohler, A., and Kulmala, M.: Hygroscopic properties of submicrometer atmospheric aerosol particles measured with H-TDMA instruments in various environments—a review, Tellus B, 60, 432-469, doi:10.1111/j.1600-0889.2008.00350.x, 2008.

Tritscher, T., Jurányi, Z., Martin, M., Chirico, R., Gysel, M., Heringa, M. F., DeCarlo, P. F., Sierau, B., Prévôt, A. S. H., Weingartner, E., and Baltensperger, U.: Changes of hygroscopicity and morphology during ageing of diesel soot, Environ. Res. Lett., 6, 034026, doi:10.1088/1748-9326/6/3/034026, 2011.

Wang, G. H., Zhang, R. Y., Gomez, M. E., Yang, L. X., Zamora, M. L., Hu, M., Lin, Y., Peng, J. F., Guo, S., Meng, J. J., Li, J. J., Cheng, C. L., Hu, T. F., Ren, Y. Q., Wang, Y. S., Gao, J., Cao, J. J., An, Z. S., Zhou, W. J., Li, G. H., Wang, J. Y., Tian, P. F., Marrero-Ortiz, W., Secrest, J., Du, Z. F., Zheng, J., Shang, D. J., Zeng, L. M., Shao, M., Wang, W. G., Huang, Y., Wang, Y., Zhu, Y. J., Li, Y. X., Hu, J. X., Pan, B., Cai, L., Cheng, Y. T., Ji, Y. M., Zhang, F., Rosenfeld, D., Liss, P. S., Duce, R. A., Kolb, C. E., and Molina, M. J.: Persistent sulfate formation from London Fog to Chinese haze, P. Natl. Acad. Sci. USA, 113, 13630-13635, doi:10.1073/pnas.1616540113, 2016.

Wang, L., Khalizov, A. F., Zheng, J., Xu, W., Ma, Y., Lal, V., and Zhang, R. Y.: Atmospheric

nanoparticles formed from heterogeneous reactions of organics, Nat. Geosci., 3, 238-242, doi:10.1038/NGEO778, 2010.

Wang, Y., Wan, Q., Meng, W., Liao, F., Tan, H., and Zhang, R.: Long-term impacts of aerosols on precipitation and lightning over the Pearl River Delta megacity area in China, Atmos. Chem. Phys. 11, 12421–12436, 2011.

Wang, Y., Khalizov, A., Levy, M., and Zhang, R.: Light absorbing aerosols and their atmospheric impacts, Atmos. Environ. 81, 713-715, doi:10.1016/j.atmosenv.2013.09.034, 2013.

Weingartner, E., Burtscher, H., and Baltensperger, U.: Hygroscopic properties of carbon and diesel soot particles, Atmos. Environ., 31, 2311-2327, doi:10.1016/S1352-2310(97)00023-X, 1997.

Wittbom, C., Eriksson, A. C., Rissler, J., Carlsson, J. E., Roldin, P., Nordin, E. Z., Nilsson, P. T., Swietlicki, E., Pagels, J. H., and Svenningsson, B.: Cloud droplet activity changes of soot aerosol upon smog chamber ageing, Atmos. Chem. Phys., 14, 9831-9854, doi:10.5194/acp-14-9831-2014, 2014.

Wu, Z. J., Zheng, J., Shang, D. J., Du, Z. F., Wu, Y. S., Zeng, L. M., Wiedensohler, A., and Hu, M.: Particle hygroscopicity and its link to chemical composition in the urban atmosphere of Beijing, China, during summertime, Atmos. Chem. Phys., 16, 1123-1138, doi:10.5194/acp-16-1123-2016, 2016.

Xue, H., Khalizov, A. F., Wang, L., Zheng, J., and Zhang, R.: Effects of dicarboxylic acid coating on the optical properties of soot, Phys. Chem. Chem. Phys., 11, 7865-7875, doi:10.1039/b700001a, 2009a.

Xue, H., Khalizov. A F., and Zhang, R.: Effects of coating of dicarboxylic acids on the mass-mobility relationship of soot particles, Environ. Sci. Technol. 43, 2787–2792, doi: 10.1021/es803287v, 2009b.

Yuan, T., Li, Z., Zhang, R., and Fan, J.: Increase of cloud droplet size with aerosol optical depth: An observation and modeling study, J. Geophys. Res., 113, D04201, doi:10.1029/2007JD008632, 2008.

Zhang, D., and Zhang R.: Laboratory investigation of heterogeneous interaction of sulfuric acid with soot, Environ. Sci. Technol. 39, 5722-5727, doi:10.1021/es050372d, 2005.

Zhang, R., Khalizov, A. F., Pagels, J., Zhang, D., Xue, H., and McMurry, P. H.: Variability in morphology, hygroscopicity, and optical properties of soot aerosols during atmospheric processing, P. Natl. Acad. Sci. USA, 105, 10291-10296, doi:10.1073/pnas.0804860105, 2008.

Zhang, R. Y., Suh, I., Zhao, J., Zhang, D., Fortner, E. C., Tie, X. X., Molina, L. T., and Molina, M. J.: Atmospheric new particle formation enhanced by organic acids, Science, 304, 1487-1490, doi:10.1126/science.1095139, 2004.

Zhang, R., Khalizov, A.F., Wang, L., Hu, M., Xu, W.: Nucleation and growth of nanoparticles in the atmosphere, Chem. Rev., 112, 1957-2011, doi:10.1021/cr2001756, 2012.

Zhang, R. Y., Wang, G. H., Guo, S., Zarnora, M. L., Ying, Q., Lin, Y., Wang, W. G., Hu, M., and Wang, Y.: Formation of Urban Fine Particulate Matter, Chem. Rev., 115, 3803-3855, doi:10.1021/acs.chemrev.5b00067, 2015.

Zhao, J., Levitt, N. P., Zhang, R., and Chen, J.: Heterogeneous reactions of methylglyoxal in acidic media: Implications for secondary organic aerosol formation, Environ. Sci.

767   Technol., 40, 7682-7687, doi:10.1021/es060610k, 2006.

768   Zhao, J., Khalizov, A.F., Zhang, R., and McGraw, R.: Hydrogen bonding interaction of
769   molecular complexes and clusters of aerosol nucleation precursors, J. Phys. Chem., 113,
770   680–689, doi:10.1021/jp806693r, 2009.

771   Zhao, P. S., Dong, F., He, D., Zhao, X. J., Zhang, X. L., Zhang, W. Z., Yao, Q., and Liu, H. Y.:
772   Characteristics of concentrations and chemical compositions for PM2.5 in the region of
773   Beijing, Tianjin, and Hebei, China, Atmos. Chem. Phys., 13, 4631-4644,
774   doi:10.5194/acp-13-4631-2013, 2013.

775   Zheng, J., Zhang, R., Fortner, E. C., Volkamer, R. M., Molina, L., Aiken, A. C., Jimenez, J. L.,
776   Gaeggeler, K., Dommen, J., Dusanter, S., Stevens, P.S., and Tie, X.: Measurements of
777   HNO_3 and N_2O_5 using ion drift - chemical ionization mass spectrometry during the
778   MCMA - 2006 campaign, Atmos. Chem. Phys., 8, 6823–6838, 2008.

779   Zheng, J., Khalizov, A., Wang, L., and Zhang, R. Y.: Atmospheric Pressure-Ion Drift
780   Chemical Ionization Mass Spectrometry for Detection of Trace Gas Species, Anal. Chem.,
781   82, 7302-7308, doi:10.1021/ac101253n, 2010.

Table 1. Summary of ambient conditions for BC aging experiments conducted in Beijing. The $PM_{2.5}$, gas concentrations and meteorological condition were averaged from the entire experimental time. D_m and T represent the mobility diameter and temperature, respectively.

No.	Date	Time		Initial D_m	$PM_{2.5}$	$J(O^1D)$	Gas Concentration (ppb)					Meteorological Conditions	
		Start	End	(nm)	($\mu g\ m^{-3}$)	(10^{-6})	Toluene	Xylene	SO_2	NO_x	O_3	T (°C)	RH (%)
#1	Aug. 18th	12:41	14:47	95	43	19	0.49	0.13	1.7	8.8	56	35	27
#2	Aug. 22nd	13:32	16:51	96	69	3.7	3.41	0.78	2	36.1	26	26	69
#3	Sep. 7th	12:40	14:52	97	12	17.5	0.71	0.17	2.7	10.2	75	30	35
#4	Sep. 9th	13:13	17:06	97	40	6.3	0.77	0.21	4	11	68	26	50
#5	Sep. 1st	13:19	16:13	147	27	11.6	0.76	0.19	4.6	19.9	83	31	33
#6	Sep. 11st	13:50	17:25	147	57	6.1	1.57	0.39	6.7	17.1	92	29	42
#7	Sep. 21st	15:31	17:41	146	30	2.1	0.75	0.29	2	10.6	90	28	37
#8	Aug. 24th	11:37	16:06	216	8.8	21.1	0.98	0.3	1.7	15.6	57	36	25
#9	Sep. 5th	14:06	16:44	220	12	8.3	0.45	0.2	2.2	14.6	54	29	35
#10	Oct. 17th	12:54	17:13	224	57	3.2	-	-	13.8	41	34	18	30

Table 2. Summary of particle properties for BC aging experiments conducted in Beijing. D_m, ρ_{eff} and D_{me} represent the mobility diameter, effective density and mass equivalent diameter, respectively.

| No. | Date | D_m | | ρ_{eff} | | D_{me} | | | |
		Initial (nm)	Final (nm)	Initial (g cm^{-3})	Final (g cm^{-3})	Initial (nm)	Final (nm)	ΔD_{me} (nm)	Growth Rate[a] (nm h^{-1})
#1	Aug. 18th	95	157	0.50	1.35	62	162	100	47
#2	Aug. 22nd	96	129	0.46	1.31	61	126	65	20
#3	Sep. 7th	97	147	0.45	1.25	62	142	80	36
#4	Sep. 9th	97	136	0.43	1.30	61	133	62	19
#5	Sep. 1st	147	170	0.34	1.36	85	168	83	29
#6	Sep. 11st	147	162	0.34	1.34	84	159	75	20
#7	Sep. 21st	146	132	0.34	1.05	84	116	32	15
#8	Aug. 24th	216	272	0.32	1.37	123	275	152	34
#9	Sep. 5th	220	202	0.25	1.33	114	197	83	31
#10	Oct. 17th	224	224	0.24	0.52	117	157	40	11
	Average							77±33	26±11

[a] The growth rate is calculated using the data between 12:00 and 17:00 for each experiment.
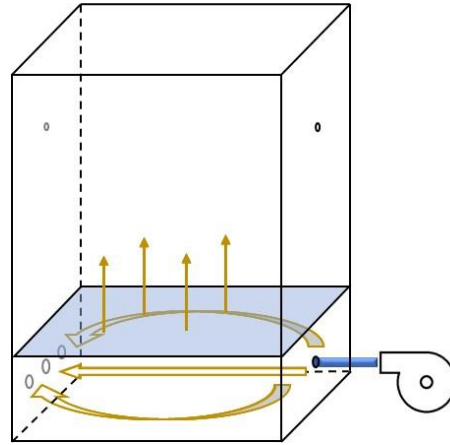
Figure 1. Photo (left) and schematic (right) of the quasi-atmospheric aerosol evolution study (QUALITY) chamber
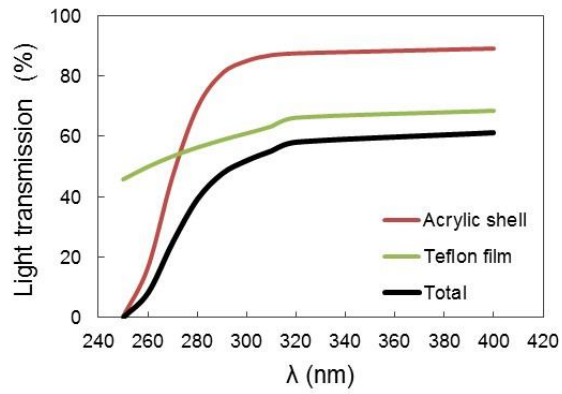
Figure 2. Light transmission spectra of the PFA Teflon film (yellow line), the acrylite shell (red line), and their total transmission in the UV range (black line).
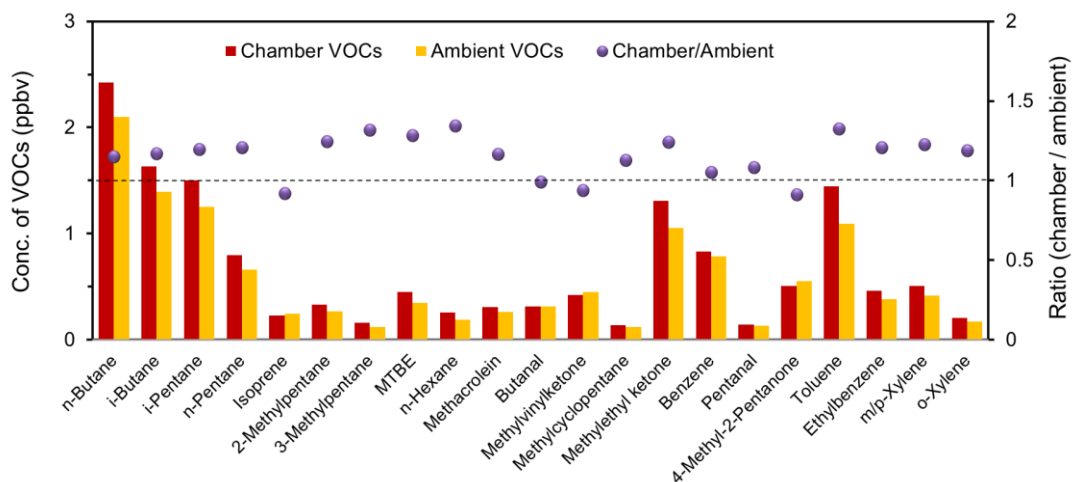
Figure 3. Comparison of VOCs concentrations in the QUALITY chamber (red bar) and in the ambient air (yellow bar) before the start of BC aging experiment. Purple cycles represent the ratio of each species in the reaction chamber to in the ambient air. Only the VOCs species that contains 4 or more carbons with the concentration higher than 0.1 ppb are shown in the figure.
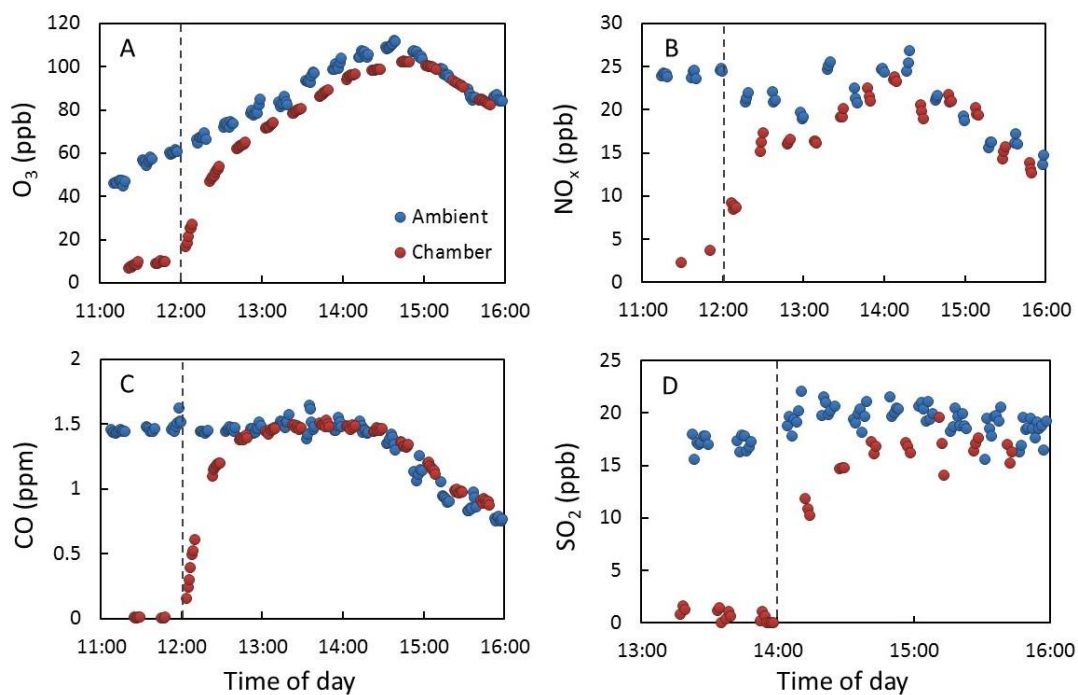
Figure 4. Concentrations of O_3 (A), NO_x (B), CO (C), and SO_2 (D) measured inside the QUALITY chamber (Red circles) and in the ambient air (blue circles). The vertical dashed lines denote the time when the ambient air started to be pulled through the bottom flow chamber and the ambient gases began to exchange into the upper reaction chamber.
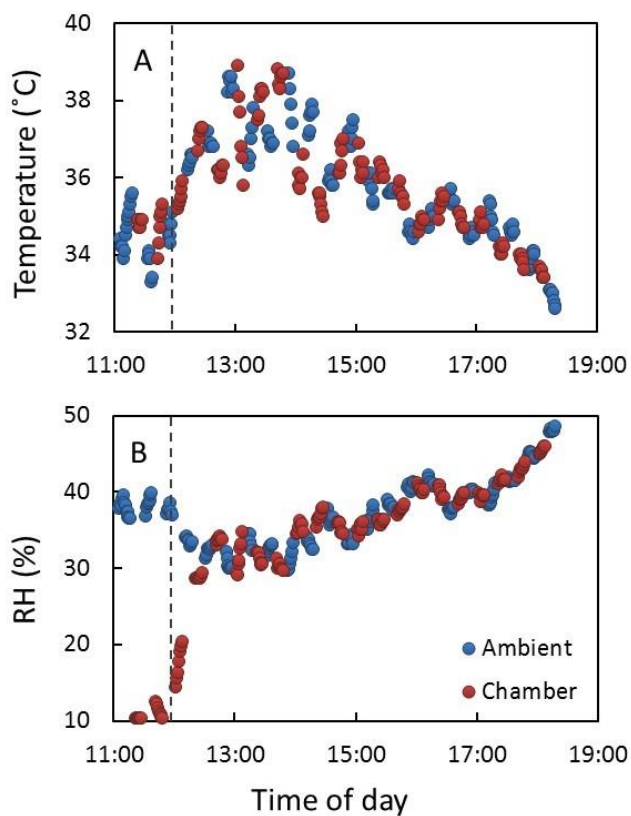
Figure 5. Temperature (A) and RH (B) measured inside the QUALITY chamber (Red circles) and in the ambient air (blue circles). The temperature and RH were measured by probes placed in the sampling tube adjacent to the chamber. The vertical dashed lines denote the time when the ambient air started to be pulled through the bottom flow chamber and the ambient gases began to exchange into the upper reaction chamber.
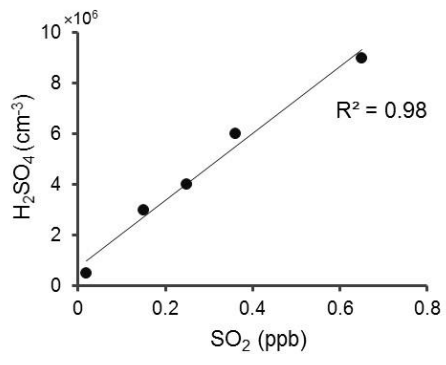
Figure 6. Sulfuric acid concentration as function of SO_2 concentration inside the chamber
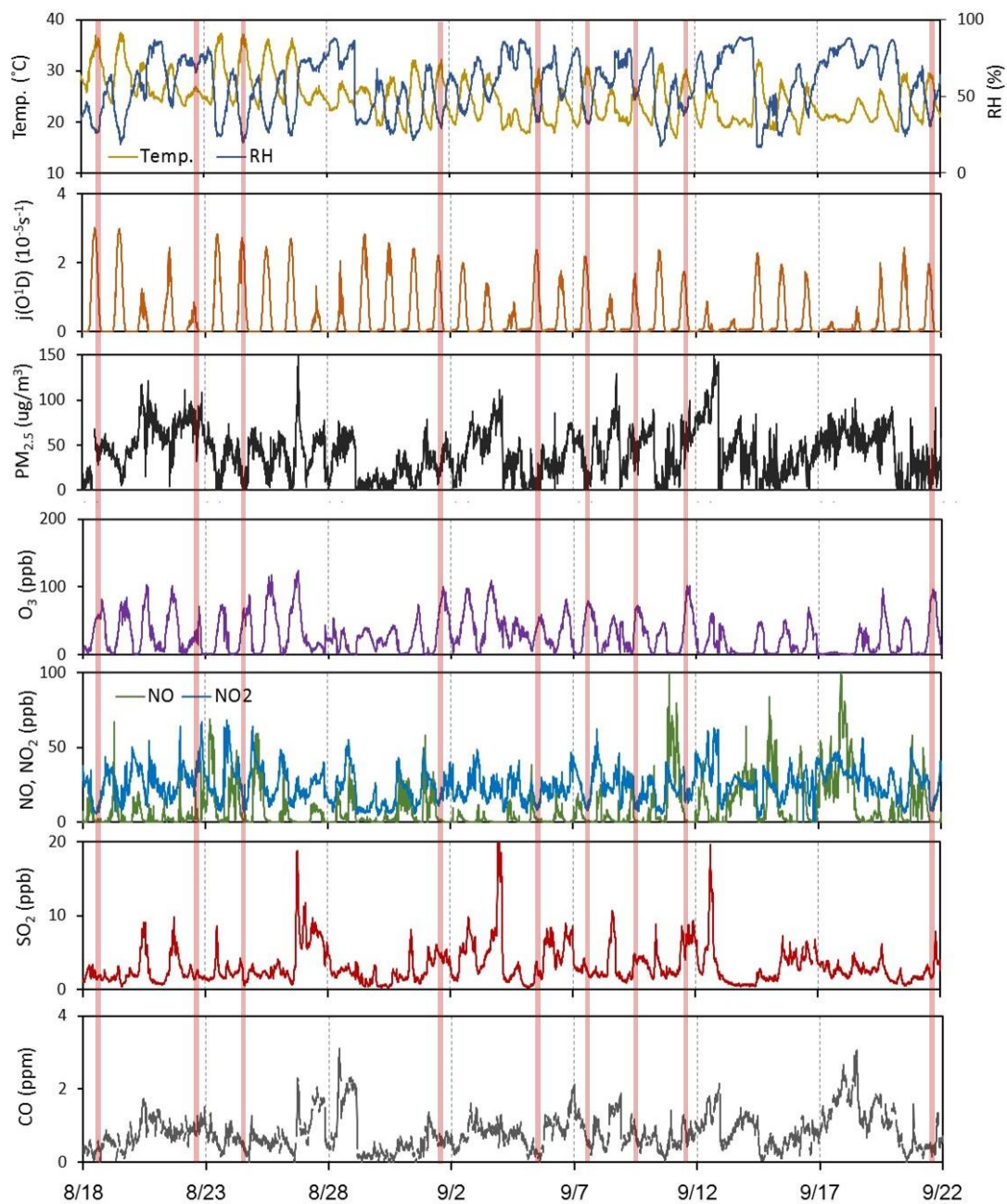
Figure 7. Time series of ambient pollutant concentrations and meteorological parameters during the experimental period in Beijing. Red bars indicate periods when BC aging experiments were conducted.
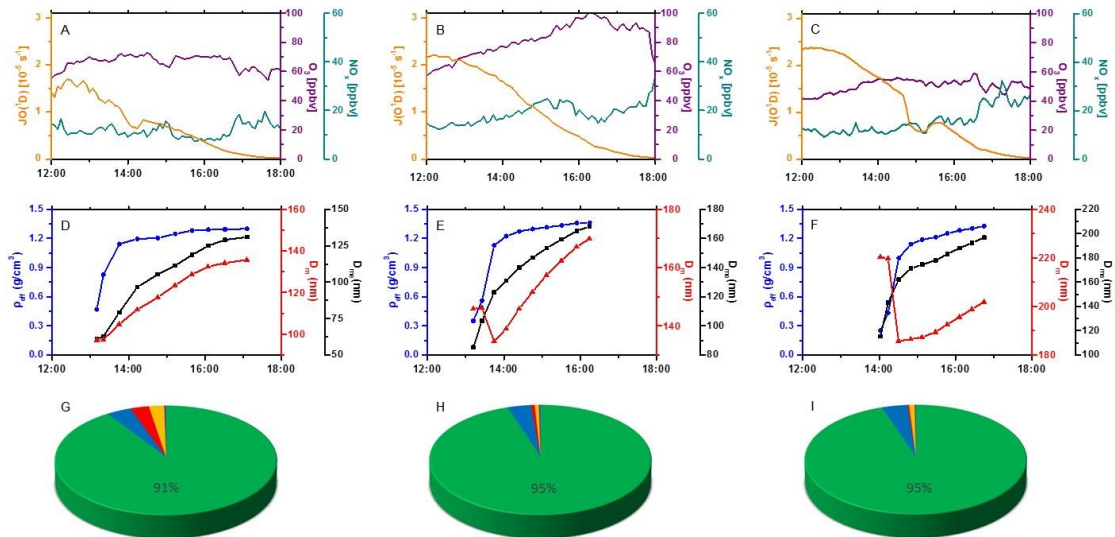
Figure 8. Ambient condition (A, B，C), changes of diameter and density of BC particle (D, E, F), and the chemical composition of coating materials (G, H, I) during three typical aging experiments. A and D correspond to experiment #4; B and E correspond to experiment #5, and C and E correspond to experiment #9. D_m is the peak mobility diameter of BC particles, ρ_{eff} is the best-fit effective density of BC particles with the mobility diameter D_m, D_{me} is the mass equivalent diameter of BC particles, and $J(O^1D)$ represents the measured photolysis rate constant for $O(^1D)$. The colors of green, blue, red, yellow and purple in the pie charts represent organics, nitrate, sulfate, ammonium, and chlorine, respectively. The numbers in figure G, H and I are the mass fraction of organics.
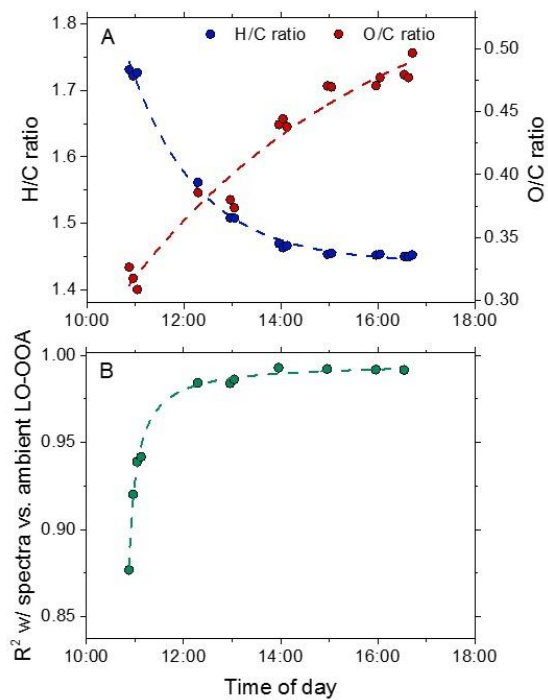
Figure 9. The evolution of organic aerosols inside the chamber during an aging experiment (#8) in Beijing. (A) the H/C and O/C ratios of organics on aged BC particles; (b) the correlation coefficients (R^2) between the evolving total OA spectra in chamber experiment and the LO-OOA spectra derived from the Beijing field data set.
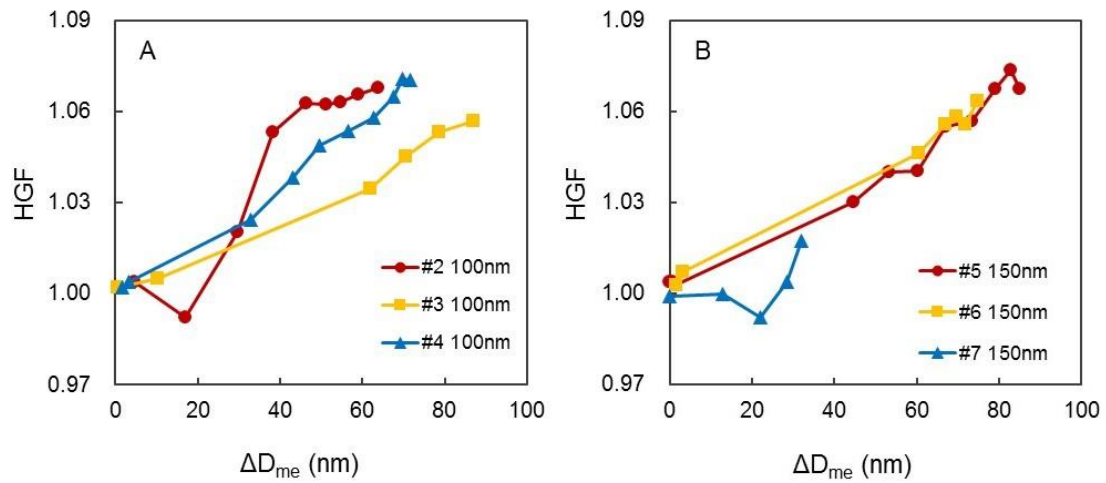
Figure 10. Evolution of hygroscopic growth factors (HGF) of BC particles during aging as a function of ΔD_{me}. (A) three experiments with 100 nm BC particle; (B) three experiments with 150 nm BC particle. Different colors in each figure represent different experiments. Hygroscopicity measurement is not available for experiment #1.
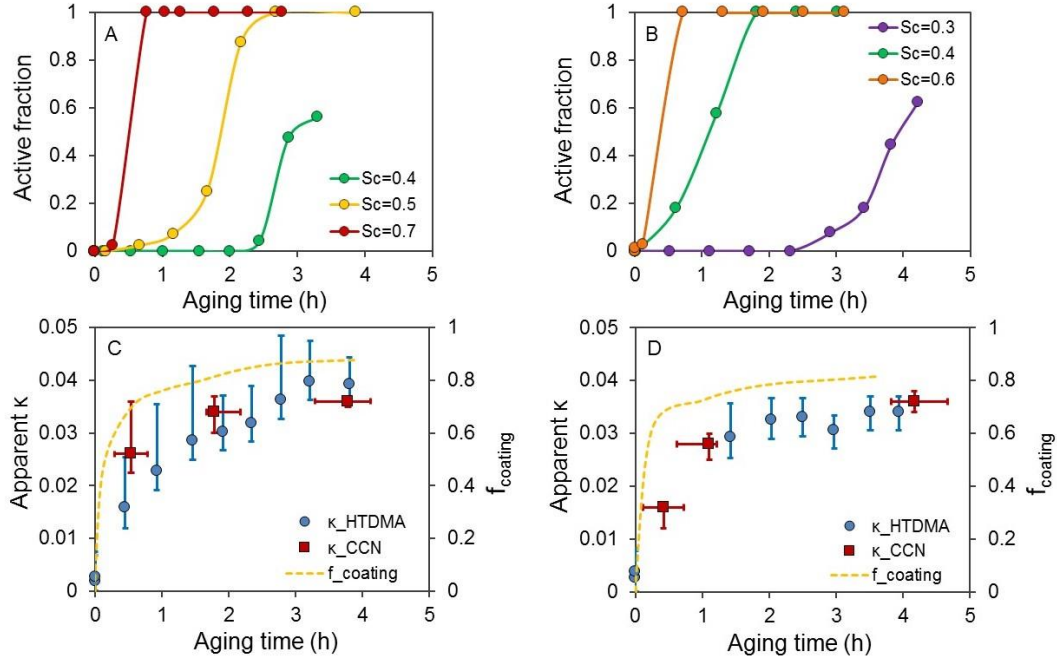
Figure 11. The active fraction of BC particles under diversified supersaturation (A, B) and the closure of apparent κ for BC particles with initial diameter (C, D) during aging in two typical experiments. A, C are the results from experiment #4 with 100nm BC particles and B, D represents experiment #6 with 150nm BC particles. Red squre and blue circle in C and D represent the apparent κ calculated using CCN counter data and HTDMA data, respectively. Yellow slash line represents the fraction of coating materials on BC particles. The error bars of κ_CCN and κ_HTDMA represent the uncertainty in the calculation.